

Multiple Ionization of Neon under soft x-rays: Theory vs Experiment

G M Nikolopoulos¹ and P Lambropoulos^{1,2}

¹Institute of Electronic Structure & Laser, FORTH, P.O.Box 1527, GR-71110
Heraklion, Greece

²Department of Physics, University of Crete, P.O. Box 2208, GR-71003 Heraklion,
Crete, Greece

Abstract.

We present a rather elaborate theoretical model describing the dynamics of Neon under radiation of photon energies ~ 93 eV and pulse duration in the range of 15 fs, within the framework of Lowest non-vanishing Order of Perturbation Theory (LOPT), cast in terms of rate equations. Our model includes sequential as well as direct multiple ionization channels from the 2s and 2p atomic shells, including aspects of fine structure, whereas the stochastic nature of SASE-FEL light pulses is also taken into account. Our predictions for the ionization yields of the different ionic species are in excellent agreement with the related experimental observations at FLASH.

1. Introduction

In a 2011 paper [1], we explored the conditions under which direct multiple ionization channels might make significant contribution to ionic yields, which are usually dominated by the inevitably present sequential channels. In order to present a quantitative assessment, we had chosen the Neon atom driven by radiation of photon energy 93 eV, of pulse intensity and duration available at present day Free-Electron Laser (FEL) facilities such as FLASH [2, 3]. Our choice was motivated in part by related experimental data obtained under the above mentioned conditions [3, 4]. Since the chief objective of our study was the evaluation of direct multiple ionization in comparison to the sequential contributions, we focused our model on the ionization of outer subshell (2p) electrons, although a complete theoretical description would have required the inclusion of single-photon ionization of 2s electrons as well. This means that we were evaluating the relative importance of direct multiple ionization from the 2p subshell alone. In a sense, our work could be viewed as a numerical experiment. At the time of that work, we were aware of only TOF (Time of Flight) data [4] which we did consider in the spirit of a qualitative comparison with our calculations; because extracting ionic yields from a figure showing TOF spikes only is highly problematic. Given its limited scope, that comparison was nevertheless compatible with our results, in the sense that under the parameters of that experiment (in particular the pulse duration), we did not expect a discernible presence of contributions from the direct channels; and indeed none was found in the experimental data. It did, however, transpire that direct multielectron channels can begin competing with the sequential ones only when the duration of the pulse falls below 5 fs or so.

In a most recent paper by Guichard et al. [5] addressing the same problem, the authors have presented a quantitative interpretation of the experimental data pertaining to the above mentioned experiment, including this time laser intensity dependences of the ionic yields. This new piece of experimental evidence behoves us to test our approach in a suitably more elaborate model. The approach in Ref. [5] relies on a rather simplified model, referred to by the authors as “minimal model”, in terms of which a good fit to the experimental data was obtained. That fit was compared (see Fig.3 of Ref. [5]) to what our equations would have given. Not surprisingly, our equations lead to ionic yields systematically lower than the experimental data. That was to be expected since, for the reasons outlined above, the single-photon ionization channels of the 2s electrons had not been taken into account in [1]. Moreover, in [5] the authors compared the experimental data to our results of Ref. [1], for a Fourier-limited pulse duration of 30 fs, which however is considerably longer than the estimated pulse duration in the experiment i.e., 15 ± 5 fs.

Since the term “minimal model” may be open to a variety of interpretations, it is important to state and discuss here clearly the main assumptions underlying the model of Ref. [5]. The formalism rests on a set of rate equations governing the production and depletion of the ionic yields during the pulse. For the photon energy, range of intensities

and pulse duration employed in the experiment, the rate equations are perfectly valid (e.g., see discussion in [1, 6, 7]). The distribution of the laser intensity within the interaction volume, as determined by the focusing geometry of the laser beam, has been taken into account. Presumably, the term “minimal model” has to do with the following additional assumptions/approximations adopted by the authors: (a) Only sequential channels were included in the rate equations. (b) The field (intensity) fluctuations, inherent in SASE FELs, and specifically FLASH pulses [2, 3, 8], were not included in the calculations. (c) All ionic species were assumed to be produced by single-photon ionization. (d) All of the single-photon cross sections entering the model were assumed to have the same value.

If the purpose of the work in [5] was to obtain a fit to the data, it appears that it has succeeded reasonably well, for the ionic species up to Ne^{4+} . However, in order to understand the physical meaning of the fit, we need to examine the validity of the underlying assumptions/approximations. Approximation (a) above is justified, because the direct channels, being of much higher order of non-linearity, are expected to begin competing with the sequential only for quite short pulses; say below 5 fs, as demonstrated in [1]. Approximation (b) may be useful in assessing some general features of the data, but the results may at times be misleading. Approximations (c) and (d), however, are quite problematic. The difficulty stems from the fact that the rate equations, which bears repeating are perfectly valid in this context, imply energy conservation in terms of number of photons absorbed in each transition and the corresponding ionization threshold. This is a condition inherent in the notion of the cross section. Thus, as discussed in detail below, although ions up to Ne^{4+} are produced mainly in a sequence of single-photon absorptions, from there on it is only two- and three-photon processes that enter the sequence of allowed transitions. In the absence of those channels, ionic species beyond Ne^{4+} cannot be populated through energy conserving processes. Inserting single-photon cross sections for those species and adjusting parameters may of course produce populations for those species, but the underlying process is devoid of physical meaning.

Coming now to the present formulation, the main addition to our earlier paper [1] is the detailed inclusion of all single-photon channels, as well as a careful estimation of the two- and three-photon cross sections. But perhaps more importantly, accounting for the field fluctuations, is shown to be of crucial importance in the interpretation of the experimental data. As has been shown in great detail in [9], for a quantitative comparison with experimental data pertaining to SASE-FEL radiation, it is imperative to include a stochastic model that describes accurately the statistical properties of the pulses, pertaining to the source and the conditions of the experiment. This is an issue sufficiently important to merit further elaboration at this point. In the absence of intensity fluctuations, it is basically the laser bandwidth that matters. In that case, for a pulsed source, the effective bandwidth is determined by the combination of the Fourier and the stochastic bandwidths. But for a source with intensity fluctuations, the particular statistics underlying the fluctuations are of crucial importance. Intensity fluctuations entail a spiky temporal structure, under an envelop determined by the pulse

duration and the usually present monochromator. As a consequence of the intensity fluctuations, an important parameter is the coherence time, which can be and often has been determined through the measurement of a two-photon autocorrelation function [8]. In essence, it provides a measure of the duration of the dominant intensity spike under the complicated spiky structure of a pulse with the stochastic properties of the SASE FEL. There is then an overall (total) bandwidth associated with this coherence time which for a Gaussian pulse and Gaussian correlated noise is given by [9]

$$\Delta\omega = \sqrt{\Delta\omega_{\min}^2 + \gamma^2}, \quad (1)$$

where $\Delta\omega_{\min}$ is the Fourier-limited bandwidth of the pulse and $\gamma = \sqrt{8\pi \ln(2)/T_c}$. In general, one cannot account for this bandwidth e.g., by simply correcting the parameters entering the equation of motion for the density matrix of the atomic system [9]. That is why detailed modelling of the field fluctuations is an absolutely necessary ingredient of the rate equations, which as a result are stochastic differential equations[9].

In the following section 2, we present a detailed discussion of the ionization channels and the respective orders of non-linearity, included in our calculations. The 1s electrons are assumed frozen because, for photon energy 93 eV and peak intensities less than $10^{16}\text{W}/\text{cm}^2$ the 1s electrons are too strongly bound to be affected. The details of the rate equations, including the interaction volume features are presented in section 3, followed by section 4 in which we present results without and with field fluctuations, thus demonstrating their significance in interpreting experimental data. In the last section 5, we summarize our findings as well as certain issues that remain open.

2. Ionization paths for Neon at 93eV

A concise summary of all ionization channels included in our calculations is shown in Fig. 1, listing important quantities, such as ionization potentials and the order of each transition, together with the flow of charge indicated by arrows. This ‘‘flow chart’’ includes ejections of electrons from both the 2s and 2p shells, where each circle corresponds to a particular ionic species with the two numbers in its lower half denoting the number of remaining electrons in the 2s and the 2p shells. This is because ionic species at different internal states appear and disappear during the ionization of neutral Neon at the particular photon energy. For example, one can see that Ne^{3+} appears in three different states, namely $|2s^2, 2p^3\rangle$, $|2s^1, 2p^4\rangle$ and $|2s^0, 2p^5\rangle$. As will be seen later on, in a sequential ionization process, a given ion at different internal states may lead to the same or to different internal states of the next higher ion, through substantially different cross-sections. For a quantitative comparison to experimental data, the inclusion of all of these intermediate ionic species is therefore necessary. In the following, the ion Ne^{q+} in the state $|2s^a, 2p^b\rangle$ is denoted by $\text{Ne}_{a,b}^{q+}$, while charge conservation implies

$$a + b = 8 - q \equiv \tilde{q}. \quad (2)$$

In view of Eq. (2), each ionic species is uniquely defined by the two labels a and b .

Careful inspection of the “flow chart” does reveal some interesting regularities in the underlying processes, which will help us elucidate the results. More precisely, for the ions up to Ne^{4+} single-photon and two-photon sequential ionization channels co-exist. On the other hand, the ions Ne^{5+} and Ne^{6+} can be created only through two-photon sequential ionization, whereas three photons are required for the last two ionic species, namely, Ne^{7+} and Ne^{8+} . The direct multiple ionization channels depicted in Fig. 1 lead from Ne to Ne^{q+} , with $q \geq 2$, and pertain to the multiphoton ejection of more than one electrons from the 2p shell of neutral Neon only, since channels that involve electron ejection from the 2s shell are expected to have considerably smaller cross sections. In principle, when energetically allowed, n -photon m -electron ejection (with $n \geq m$) can always occur from any ionic species, and actually it does not necessarily require any electron correlation. As a first approximation, however, we have included only direct ionization channels from neutral Neon, since this is mainly present for short times. Our simulations, showed that for the parameters of the experiment, the contribution of these channels was negligible and thus there was no need for including direct ionization of intermediate ions.

Finally, it should be emphasized that the “flow chart” of Fig. 1 corresponds to photon energy 93 eV, with the ionization potentials obtained from the codes in Ref. [10]. The counterpart of this “flow chart” for photon energy 90.5 eV differs only in the order of the transition $\text{Ne}_{2,4}^{2+} \rightarrow \text{Ne}_{1,4}^{3+}$, which becomes a two-photon process. In either case, it is the ratio of the cross sections for the transitions $\text{Ne}_{2,4}^{2+} \rightarrow \text{Ne}_{2,3}^{3+}$ and $\text{Ne}_{2,4}^{2+} \rightarrow \text{Ne}_{1,4}^{3+}$ that determines the dominant ionization path followed by the system. As shown in Table A1, the single-photon cross-section for $\text{Ne}_{2,4}^{2+} \rightarrow \text{Ne}_{2,3}^{3+}$ at 93 eV is considerably larger than the corresponding cross-section for $\text{Ne}_{2,4}^{2+} \rightarrow \text{Ne}_{1,4}^{3+}$. Moreover, as discussed later on, the manifold of (near) resonances at 90.5 and 93 eV are very similar, and thus the relative strength of the cross sections remain practically the same. Therefore, considering either of the photon energies reported in the experiment of [5], is not expected to modify or introduce any prominent distinguishing features in the yields of Ne^{2+} and Ne^{3+} , in agreement with the reported experimental data. As a result, for the sake of concreteness, our theoretical analysis has been focused on photons of energy 93 eV. As confirmed later on, our theoretical results for the laser intensity dependence of the ionic yields are in a very good agreement with those of the experiment for both 90.5 and 93 eV.

3. Theory vs Experiment

As discussed above, our model focuses on the populations of the ionic species up to Ne^{8+} and includes different sequential and direct ionization paths from both of the 2s and 2p shells. Although in the experimental data, the highest observable ionic species was Ne^{6+} , it is necessary to include the rate equations for Ne^{7+} and Ne^{8+} , because otherwise the population of Ne^{6+} would increase monotonically, reaching eventually the value 1, violating thus the physical reality of the experiment. Throughout our simulations, the

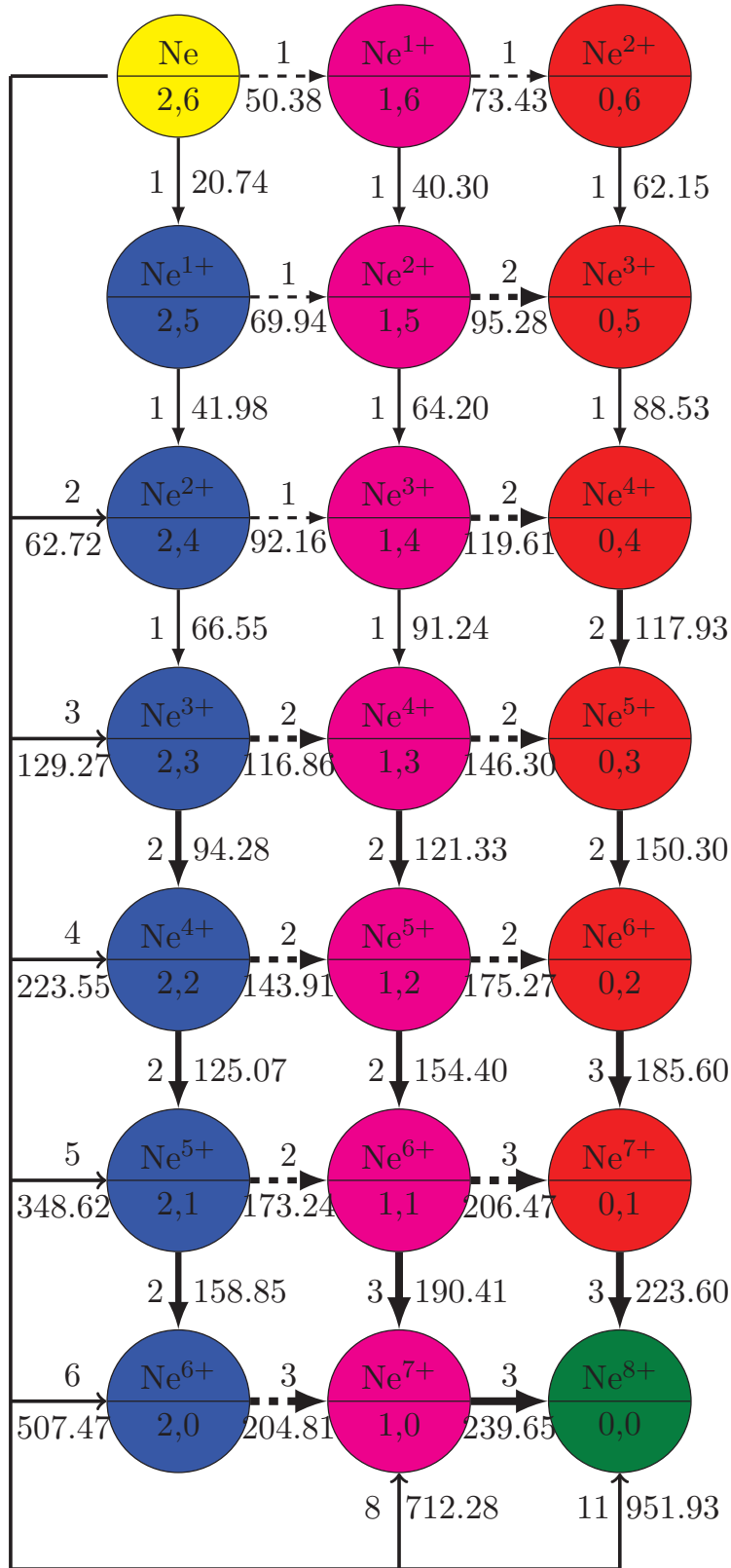


Figure 1. Ionization paths for Neon. The numbers close to each arrow denote the ionization potential in eV and the number of photons required for ionization assuming photons of energy 93 eV. Different colours (columns) denote ion species with 0, 1 and 2 holes in the 2s shell.

complete set of differential equations that governs the populations of the ionic species during the pulse is the following:

$$\begin{aligned} \frac{dN_{2,6}}{dt} = & -\sigma_{2,6;1,6}^{(1)}FN_{2,6} - \sigma_{2,6;2,5}^{(1)}FN_{2,6} \\ & - \sum_{b=0}^4 \sigma_{2,6;2,b}^{(6-b)}F^{6-b}N_{2,6} - \sigma_{2,6;1,0}^{(8)}F^8N_{2,6} - \sigma_{2,6;0,0}^{(11)}F^{11}N_{2,6} \end{aligned} \quad (3)$$

$$\frac{dN_{2,5}}{dt} = \sigma_{2,6;2,5}^{(1)}FN_{2,6} - \sigma_{2,5;1,5}^{(1)}FN_{2,5} - \sigma_{2,5;2,4}^{(1)}FN_{2,5} \quad (4)$$

$$\frac{dN_{1,6}}{dt} = \sigma_{2,6;1,6}^{(1)}FN_{2,6} - \sigma_{1,6;0,6}^{(1)}FN_{1,6} - \sigma_{1,6;1,5}^{(1)}FN_{1,6} \quad (5)$$

$$\begin{aligned} \frac{dN_{2,4}}{dt} = & \sigma_{2,5;2,4}^{(1)}FN_{2,5} + \sigma_{2,6;2,4}^{(2)}F^2N_{2,6} \\ & - \sigma_{2,4;2,3}^{(1)}FN_{2,4} - \sigma_{2,4;1,4}^{(1)}FN_{2,4} \end{aligned} \quad (6)$$

$$\begin{aligned} \frac{dN_{1,5}}{dt} = & \sigma_{2,5;1,5}^{(1)}FN_{2,5} + \sigma_{1,6;1,5}^{(1)}FN_{1,6} \\ & - \sigma_{1,5;1,4}^{(1)}FN_{1,5} - \sigma_{1,5;0,5}^{(2)}F^2N_{1,5} \end{aligned} \quad (7)$$

$$\frac{dN_{0,6}}{dt} = \sigma_{1,6;0,6}^{(1)}FN_{1,6} - \sigma_{0,6;0,5}^{(1)}FN_{0,6} \quad (8)$$

$$\begin{aligned} \frac{dN_{2,3}}{dt} = & \sigma_{2,4;2,3}^{(1)}FN_{2,4} + \sigma_{2,6;2,3}^{(3)}F^3N_{2,6} \\ & - \sigma_{2,3;2,2}^{(2)}F^2N_{2,3} - \sigma_{2,3;1,3}^{(2)}F^2N_{2,3} \end{aligned} \quad (9)$$

$$\begin{aligned} \frac{dN_{1,4}}{dt} = & \sigma_{2,4;1,4}^{(1)}FN_{2,4} + \sigma_{1,5;1,4}^{(1)}FN_{1,5} \\ & - \sigma_{1,4;1,3}^{(1)}FN_{1,4} - \sigma_{1,4;0,4}^{(2)}F^2N_{1,4} \end{aligned} \quad (10)$$

$$\frac{dN_{0,5}}{dt} = \sigma_{0,6;0,5}^{(1)}FN_{0,6} + \sigma_{1,5;0,5}^{(2)}F^2N_{1,5} - \sigma_{0,5;0,4}^{(1)}FN_{0,5} \quad (11)$$

$$\begin{aligned} \frac{dN_{2,2}}{dt} = & \sigma_{2,3;2,2}^{(2)}F^2N_{2,3} + \sigma_{2,6;2,2}^{(4)}F^4N_{2,6} \\ & - \sigma_{2,2;2,1}^{(2)}F^2N_{2,2} - \sigma_{2,2;1,2}^{(2)}F^2N_{2,2} \end{aligned} \quad (12)$$

$$\begin{aligned} \frac{dN_{1,3}}{dt} = & \sigma_{2,3;1,3}^{(2)}F^2N_{2,3} + \sigma_{1,4;1,3}^{(1)}FN_{1,4} \\ & - \sigma_{1,3;1,2}^{(2)}F^2N_{1,3} - \sigma_{1,3;0,3}^{(2)}F^2N_{0,3} \end{aligned} \quad (13)$$

$$\frac{dN_{0,4}}{dt} = \sigma_{0,5;0,4}^{(1)}FN_{0,5} + \sigma_{1,4;0,4}^{(2)}FN_{1,4} - \sigma_{0,4;0,3}^{(2)}F^2N_{0,4} \quad (14)$$

$$\begin{aligned} \frac{dN_{2,1}}{dt} = & \sigma_{2,2;2,1}^{(2)}F^2N_{2,2} + \sigma_{2,6;2,1}^{(5)}F^5N_{2,6} \\ & - \sigma_{2,1;2,0}^{(2)}F^2N_{2,1} - \sigma_{2,1;1,1}^{(2)}F^2N_{2,1} \end{aligned} \quad (15)$$

$$\begin{aligned} \frac{dN_{1,2}}{dt} = & \sigma_{2,2;1,2}^{(2)}F^2N_{2,2} + \sigma_{1,3;1,2}^{(2)}F^2N_{1,3} \\ & - \sigma_{1,2;1,1}^{(2)}F^2N_{1,2} - \sigma_{1,2;0,2}^{(2)}F^2N_{1,2} \end{aligned} \quad (16)$$

$$\frac{dN_{0,3}}{dt} = \sigma_{0,4;0,3}^{(2)}F^2N_{0,4} + \sigma_{1,3;0,3}^{(2)}FN_{1,3} - \sigma_{0,3;0,2}^{(2)}F^2N_{0,3} \quad (17)$$

$$\frac{dN_{2,0}}{dt} = \sigma_{2,1;2,0}^{(2)} F^2 N_{2,1} + \sigma_{2,6;2,0}^{(6)} F^6 N_{2,6} - \sigma_{2,0;1,0}^{(3)} F^3 N_{2,0} \quad (18)$$

$$\begin{aligned} \frac{dN_{1,1}}{dt} = & \sigma_{2,1;1,1}^{(2)} F^2 N_{2,1} + \sigma_{1,2;1,1}^{(2)} F^2 N_{1,2} \\ & - \sigma_{1,1;1,0}^{(3)} F^3 N_{1,1} - \sigma_{1,1;0,1}^{(3)} F^3 N_{1,1} \end{aligned} \quad (19)$$

$$\frac{dN_{0,2}}{dt} = \sigma_{0,3;0,2}^{(2)} F^2 N_{0,3} + \sigma_{1,2;0,2}^{(2)} F N_{1,2} - \sigma_{0,2;0,1}^{(3)} F^3 N_{0,2} \quad (20)$$

$$\begin{aligned} \frac{dN_{1,0}}{dt} = & \sigma_{2,0;1,0}^{(3)} F^3 N_{2,0} + \sigma_{2,6;1,0}^{(8)} F^8 N_{2,6} \\ & + \sigma_{1,1;1,0}^{(3)} F^3 N_{1,1} - \sigma_{1,0;0,0}^{(3)} F^3 N_{1,0} \end{aligned} \quad (21)$$

$$\frac{dN_{0,1}}{dt} = \sigma_{0,2;0,1}^{(3)} F^3 N_{0,2} + \sigma_{1,1;0,1}^{(3)} F N_{1,1} - \sigma_{0,1;0,0}^{(3)} F^3 N_{0,1} \quad (22)$$

$$\frac{dN_{0,0}}{dt} = \sigma_{1,0;0,0}^{(3)} F^3 N_{1,0} + \sigma_{0,1;0,0}^{(3)} F^3 N_{0,1} + \sigma_{2,6;0,0}^{(11)} F^{11} N_{2,6}. \quad (23)$$

Here, $N_{a,b}$ refers to the population of the ionic species $\text{Ne}_{a,b}^{q+}$. A term like $\sigma_{a,b;a',b'}^{(n)} F^n N_{a',b'}$ represents an n -photon process leading from $\text{Ne}_{a,b}^{q+}$ to $\text{Ne}_{a',b'}^{q'+}$ with the corresponding (generalized) cross-section $\sigma_{a,b;a',b'}^{(n)}$ in units of $\text{cm}^{2n} \text{sec}^{n-1}$, while $F(t)$ is the time-dependent photon flux in photons/ $\text{cm}^2 \text{sec}$. The total ionization yield for Ne^{q+} is obtained by summing up the yields at all possible states of Ne^{q+} i.e.,

$$N_q = \sum_a N_{a,8-q-a}, \quad (24)$$

with $\max\{0, 2 - q\} \leq a \leq \min\{2, 8 - q\}$.

In setting up the rate equations, all single-photon cross sections were obtained from [10]. The values of the two- and three-photon cross sections were obtained through a combination of scaling [11] with proper accounting for the level structure of the respective species, in order to identify the possible influence of near-resonant intermediate states. The final set of cross sections employed in the calculations for photon energy at 93 eV is listed in Table A1. The reader familiar with the range of magnitudes of multiphoton ionization cross sections may notice that some of the two-photon and three-photon cross sections tend to be in the range of the larger values. This is due to the presence of intermediate near resonances some of which are given in Table A2. It should be emphasized here that the landscape of (near) resonances we have found by means of [10] at 93 eV, remains practically the same at 90.5 eV. Hence, the above set of rate equations and the associated cross-sections listed in table A1 are expected to describe equally well the ionization of Neon at both photon energies.

The closed set of rate equations (3)-(23) is to be solved under a realistic pulse, specified by the conditions in the experiment under consideration. For quantitative comparison with experimental data, however, one must take into account the spatial distribution of the laser intensity within the interaction volume. Throughout our simulations we have considered a Gaussian beam whose intensity is given by

$$I(r, z; t) = I(t) \frac{w_0^2}{w(z)^2} \exp \left[-\frac{2r^2}{w(z)^2} \right] \equiv I(t) I(r, z) \quad (25)$$

where $w(z) = w_0 \sqrt{1 + (z/z_R)^2}$ is the beam radius, z_R is the Rayleigh length and w_0 is the beam waist. The temporal profile of the intensity is also taken to be a Gaussian of the form

$$I(t) = I_0 \exp \left[-\frac{(t - t_0)^2}{\tau^2} \right], \quad (26)$$

where I_0 is the peak intensity, $t = t_0$ is the center of the pulse, and τ is the pulse duration. The FWHM of $I(t)$ is given by $2\sqrt{\ln(2)}\tau$.

The solution of the rate equations takes place on a three-dimensional grid for $(r, z; t)$, with $r \in [0, R_{\max}]$, $z \in [-Z_{\min}, Z_{\max}]$ and $t \in [0, T_f]$. For a given peak intensity I_0 , we choose a point in space (r, z) and the equations are solved numerically in time from $t = 0$ to $t = T_f$, with the initial condition $N_{2,6} = 1$ and $N_{a,b} = 0$, otherwise. The flux entering the equations is given by

$$F(r, z; t) = \frac{0.624 \times 10^{19}}{\hbar\omega_{ph}} I(r, z; t) \quad (27)$$

where the photon energy $\hbar\omega_{ph}$ is given in eV and the intensity is in W/cm². The same procedure is followed for the next spatial point, until the entire spatial grid is covered. In this way, one obtains the yields for the values of the intensity at all points on the spatial grid. Finally, performing a numerical spatial integration one obtains the total ionic yields at the chosen peak intensity I_0 .

The resulting theoretical predictions, at this point for a Gaussian Fourier-limited pulse, together with the experimental yields reported in [5] are presented in Fig. 2, for three different pulse durations. All of the parameters entering Eqs. (25) and (26) are in agreement with the ones adopted in [5]. There is an overall very good agreement with the experimental data for all species, especially for pulses with FWHM 15fs and 20fs. There is a disagreement for Ne¹⁺ at high intensities, as well as for the ions above Ne³⁺, which were also present in the comparison of the experimental data with the “minimal model” of Ref. [5]. The present theoretical model, however, produces much better agreement with the experimental data for all ions. Although in some cases the observed discrepancies are within the reported experimental uncertainties, the question arises as to whether a better agreement could be obtained in the framework of the present theoretical model under the constraint of the experimental conditions reported in [5]. Having performed extensive simulations, we have reached the conclusion that no dramatic improvement can be expected with Fourier-limited temporal pulse shapes.

To those familiar with the properties of SASE-FEL radiation, this would not come as a surprise. Because an important feature of SASE-FEL radiation, which has not been included in our model so far, is the presence of stochastic intensity fluctuations which are well represented by Gaussian-correlated noise [2, 3, 8]. As a consequence a pulse of duration τ typically exhibits a number of narrower spikes whose duration is basically associated with the so-called coherence time T_c . In fact, the coherence time at FLASH at the time of the experiments under consideration was estimated to be about 6 fs, which means that for pulse durations 15 ± 5 fs, roughly speaking there were a few spikes per pulse [2, 3, 8]. We have developed a rather efficient numerical

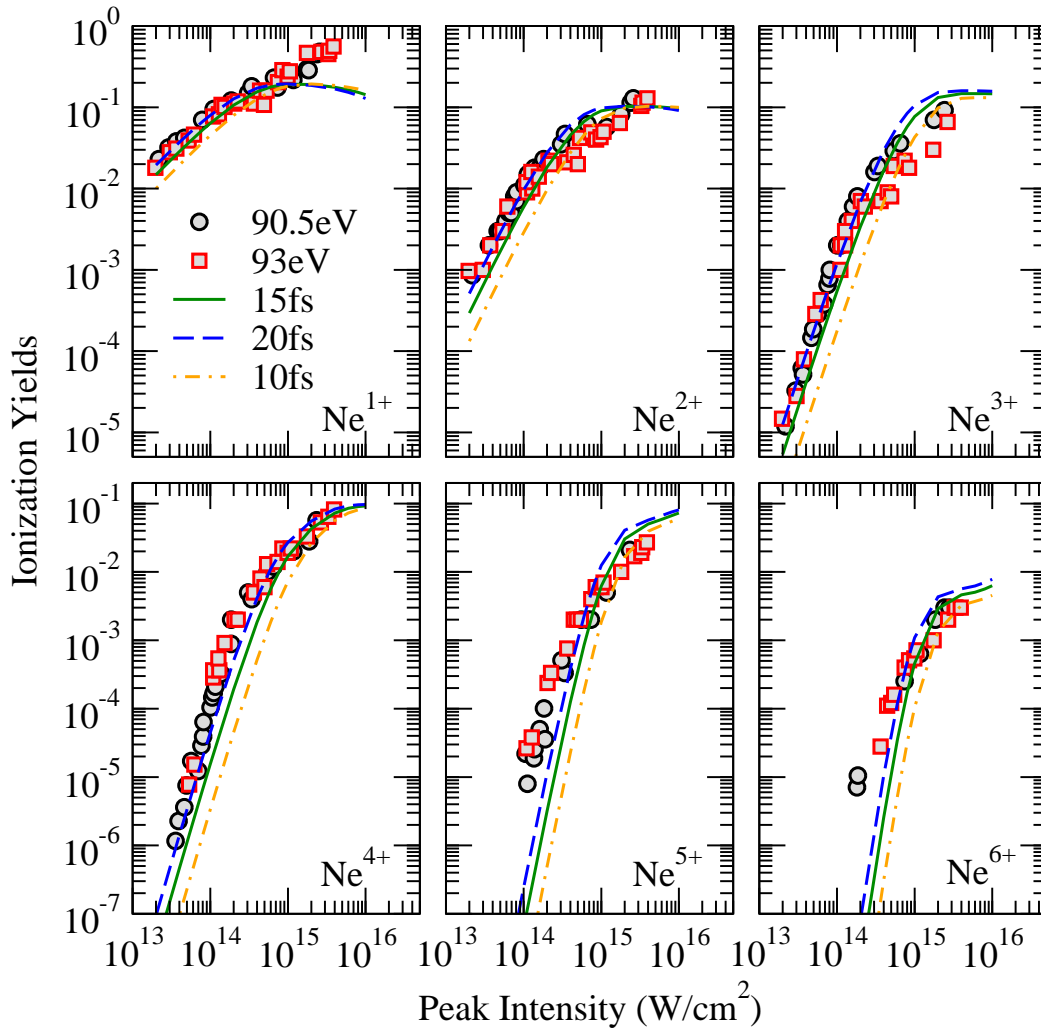


Figure 2. Experiment vs theory: Ionization yields for Neon. The symbols are experimental data for 93 and 90.5 eV, and have been extracted from [5]. The curves are theoretical results after spatial integration for Fourier-limited pulses of various durations (FWHM).

approach for the simulation of such pulses, which captures all of the essential features for the problem under consideration. For example, our approach was recently applied to the study of the line-shape of an Auger resonance in Kr [9], in excellent agreement with related experimental observations at FLASH [12]. Our numerical approach, as described in detail elsewhere [9], has been employed in this work as well, in order to address the aforementioned persistent discrepancy between theory and experiment, for Fourier-limited pulses.

In taking this step, the only thing that changes in our model is the temporal profile of the pulse entering our equations, which is no longer given by Eq. (26), but is instead a stochastic function generated numerically according to the algorithm of [9]. Under the stochastically fluctuating pulses, the equations must now be solved for a number of

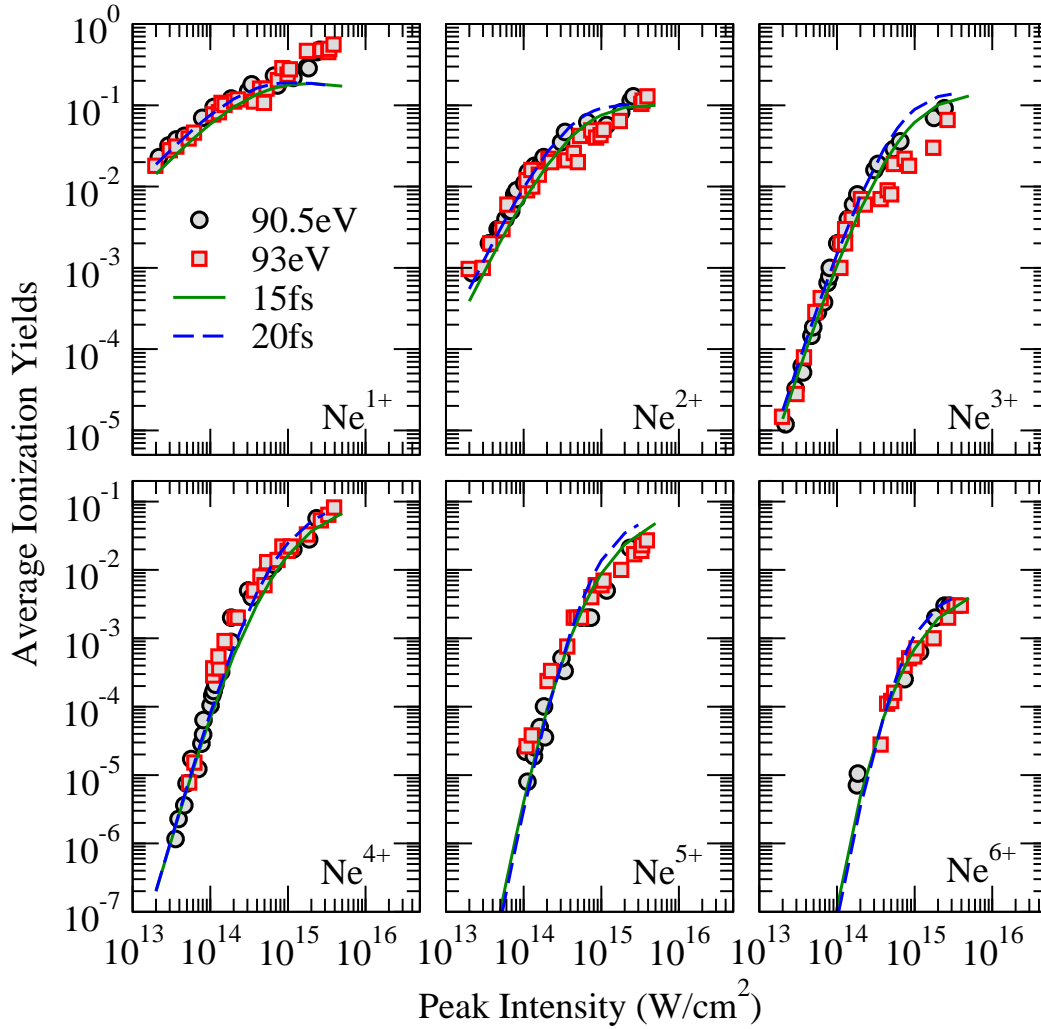


Figure 3. Experiment vs theory: Ionization yields for Neon. The symbols are experimental data for 93 and 90.5 eV, and have been extracted from [5]. The curves are theoretical results after spatial integration, averaged over 500 fluctuating pulses with $T_c = 6$ fs and two different pulse durations (FWHM).

randomly generated pulses, with the quantities of interest being the ionic yields averaged over an appropriate number of fluctuating pulses which, by the way, is exactly what is done in the collection of the experimental data. In the case under consideration, the experimental data presented in [5] were averaged over 500 consecutive FEL pulses, and we have thus chosen the same number in our simulations. As shown in Fig. 3, we obtain excellent agreement with the experimental data for all ionic species, including Ne^{5+} and Ne^{6+} . The only remaining discernible discrepancy appears for Ne^{1+} at the higher peak intensities, which is also the case in [5]. Possible reasons for this discrepancy are discussed in the section that follows.

4. Concluding remarks and discussion

Motivated by the recent work of Guichard et al. [5], we have extended our previous work on the ionization of the Neon at photon energies ~ 93 eV, in the framework of Lowest non-vanishing Order Perturbation Theory (LOPT). Aiming at an approach that can serve as an example for the interpretation of similar experiments under FEL radiation, we have endeavoured to include in the theory as much quantitative detail as possible. In that sense, our objective has been to develop an approach with predictive as well as interpretative capability. The excellent agreement between theory and experiment in the laser intensity dependence of all available ionic yields, that we have obtained, confirms the quantitative validity of LOPT [6] and the associated rate equations, incorporating sequential and if necessary direct multiple ionization channels, in the context of experiments under present day FEL sources. To this end, however, all possible atomic shells involved in the ionization have to be taken into account, with the assignment of reasonable cross sections that are consistent with the atomic structure. But that may not be enough. As we have demonstrated in this work, under SASE-FEL sources and particularly in the presence of non-linear processes, the realistic and accurate inclusion of the stochastic properties of the source, accounting for the intensity fluctuations, is mandatory for the quantitative interpretation and understanding of experimental data on multiple ionization.

We have thus grounds to argue that a quantitative interpretation of experimental data, such as those considered in this paper, which is consistent with the underlying physics, is best served by a sufficiently elaborate theoretical model. We invite the reader to contrast our fit of the higher ionic species, namely Ne^{5+} and Ne^{6+} , with that in [5]. The inadequacy of the minimal model for those ions is traceable directly to the absence of the non-linear processes beyond Ne^{4+} which are necessary for the generation of the higher ions.

A discrepancy between theory and experiment for Ne^{1+} at the higher intensity range has persisted through all of our calculations, as is also the case with the minimal model results [5]. Since the production of Ne^{1+} involves only single photon processes, with known cross sections and without any complications of atomic structure, this discrepancy is somewhat puzzling. One possible cause of this behaviour may have to do with the way data at different intensities were taken in the measurements. Usually, the intensity is decreased by inserting a linear absorber between the source and the gas chamber. In that case, the geometry of the interaction volume is the same for all intensities, and this is how it has been modelled in our theory. According to the experimental papers, however, the intensity has been controlled by moving the focal spot of the radiation from the center of the atomic beam. As we understand it, this may indeed expose most of the atoms in the gas jet to lower intensities, but at the same time the geometry of the interaction volume is altered. Having encountered this issue in much earlier work [6] on data by the same group, we have noted that some sort of volume “renormalization” must have been involved. Without access to the details of

this procedure, there is not much we can add by way of answer, other than leaving the above comments as a conjecture.

There is one additional aspect that is worth discussing in brief before closing. It has to do with the possibility that ionization plus excitation, often called also “shake up”, may leave some ions in an excited state, which can then be ionized in the next step. Let us, for the sake of clarity, take a specific example. Under photon energy of 93 eV, in addition to ejecting one 2p electron from neutral Neon, there is a single-photon two-electron process which leads to Ne^{1+} , with one electron for example in the 3d state. This process can be repeated in the next step, giving rise to an analogous excited state of Ne^{2+} . In the next step, this two-electron process is energetically forbidden. The electrons in the created excited states can be ionized by single-photon absorption. Although, we have not been able to find experimental data or theoretical calculations for these two-electron processes in Neon, from information for other atoms and molecules [12, 13, 14, 15, 16], we do know that typically the cross section for ionization plus excitation amounts to a few percent, say 2-4%, of the dominant single-photon ionization cross section of a 2p electron, which leaves the ion in the ground state. That is because such single-photon two-electron processes rely on electron correlation which is weak compared to the ejection of one electron. For pulse durations in the range of 10-50 fs, those excited states do not have the time to undergo spontaneous emission. Knowing the ionization cross sections of such excited states, which are in the range of 10^{-20} to 10^{-19}cm^2 , we can estimate rather reliably the amount of Ne^{4+} that may survive in the excited state. It is the excited state of this species that is of interest here, because the single-photon ionization of the excited electron would compete with the two-photon ionization of the ground state. Given that only a very small amount, at best no more than 2% or so, may be present during the pulse, we can calculate the laser intensity at which its ionization would compete with the two-photon process of the ground state. The result is that for intensities larger than 10^{13} W/cm^2 , the contribution of that single photon process is insignificant, in comparison to the two-photon one, even if the two-photon cross section is quite small. We should perhaps remind the reader that the rate of a single-photon process, which depends linearly, can compete with a two-photon process, which depends quadratically on the photon flux, only at lower intensities. It is nevertheless conceivable that a minute trace of those shake-up processes may be present in the data. Their identification would, however, require data well beyond the detection of ionic yields.

But even within the limits of the detection of ionic yields, there are interesting details which illustrate the interplay of various non-linear processes. One such example is shown in Fig. 4, where we have plotted ionic yields without interaction volume averaging for a Fourier-limited pulse of 15 fs. As the reader will notice, beginning with Ne^{4+} , the yields for the higher ionic species exhibit dips of increasing depth, at the higher laser peak intensities. Although the volume averaging is an experimental reality, still the detection of ionic yields, at the center of the interaction volume where the intensity is constant, is in principle possible, but much more demanding experimentally.

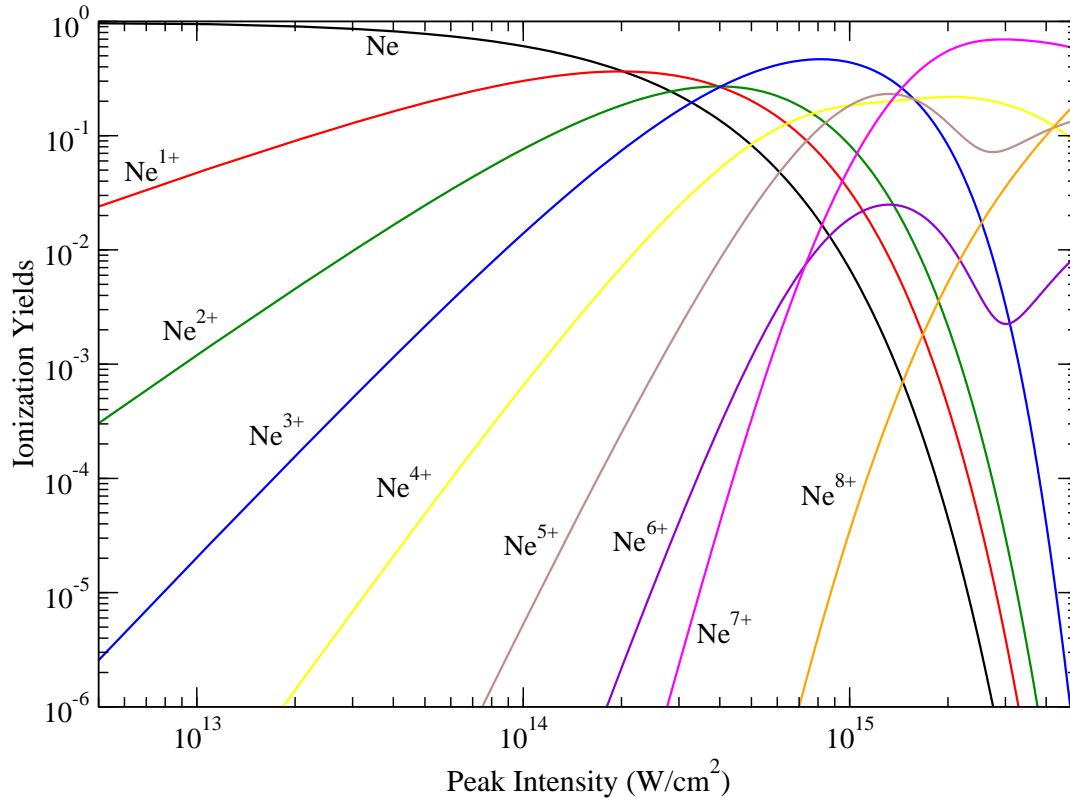


Figure 4. Ionization yields for Neon at 93 eV, for Fourier-limited pulse of FWHM 15 fs, and with no volume expansion effects.

Nevertheless having that behaviour at the theoretical level, is useful in that it does provide a point of comparison of different theoretical approaches, while at the same time illustrating details of the dynamics of the system. We do realize, as we have tested it, that the presence of fluctuations will most likely smooth out the dips appearing at relatively high intensities. On the other hand, one of the directions pursued in the continuing development of FEL sources is to reach practically Fourier-limited pulses. Thus, our example albeit idealized at this point in time, may be useful as a point of calibration in the near future.

5. Acknowledgments

The authors wish to acknowledge informative communications with the authors of [5] concerning the assumptions adopted in their model. This work was supported in part by the European COST Action CM1204 (XLIC).

Appendix A. Cross sections

Figures 2 and 3 have been produced using the cross-sections given in table A1. The single-photon cross sections entering the above equations have been obtained by means

of the codes in [10], whereas the multiphoton cross-sections have been obtained as explained in section 3 .

References

- [1] P. Lambropoulos, G. M. Nikolopoulos and K. G. Papamihail, Phys. Rev. A **83**, 021407(R) (2011).
- [2] W. Ackermann *et al.*, Nature Photonics **1**, 336 (2007); P. Emma *et al.*, Nature Photonics **4**, 641 (2010); K. Tiedke *et al.*, **11**, 023029 (2009).
- [3] A. A. Sorokin *et al.*, Phys. Rev. Lett. **99**, 213002 (2007); M. Richter *et al.* J. Phys. B: At. Mol. Opt. Phys. **43**, 194005 (2010) and references therein.
- [4] M. Richter *et al.*, Phys. Rev. Lett. **102**, 163002 (2009).
- [5] R. Gichard *et al.*, J. Phys. B: At. Mol. Opt. Phys. **46**, 164025 (2013).
- [6] M. G. Makris, P. Lambropoulos and A. Mihelic, Phys. Rev. Lett. **102**, 033002 (2009).
- [7] P. Lambropoulos and G. M. Nikolopoulos, Eur. Phys. J. Special Topics **222**, 2067 (2013).
- [8] R. Mitzner *et al.*, Optics Express **16**, 19909 (2008); R. Mitzner *et al.*, Phys. Rev. A **80**, 025402 (2009).
- [9] G. M. Nikolopoulos and P. Lambropoulos, Phys. Rev. A **86** 033420 (2012); G. M. Nikolopoulos and P. Lambropoulos, J. Phys. B: At. Mol. Opt. Phys. **46**, 164010 (2013)
- [10] Los Alamos Atom Physics Codes <http://aphysics2.lanl.gov/tempweb/lanl/>
- [11] P. Lambropoulos, Comments At. Mol. Phys. **20**, 199 (1987) and references therein; P. Lambropoulos and X. Tang, J. Opt. Soc. Am. B **4**, 821 (1987)
- [12] T. Mazza *et al.*, J. Phys. B: At. Mol. Opt. Phys. **45** 141001 (2012).
- [13] W. Wijesundera and H. P. Kelly, Phys. Rev. A **36**, 4539 (1987).
- [14] H. Kossmann *et al.* Phys. Rev. Lett. **58**, 1620 (1987).
- [15] I. Sanchez and F. Martin Phys. Rev. A **44**, 7318 (1991) and references therein.
- [16] T. Nakajima and L. A. A. Nikolopoulos Phys. Rev. A **66**, 041402(R), (2002).

Table A1. Values of the cross sections used in obtaining the figures of this work ^(a).

Cross section $\sigma_{a,b;a',b'}^{(n)}$	Value ($\text{cm}^{2n}\text{sec}^{n-1}$)
$\sigma_{2,6;2,5}^{(1)}$	4.08×10^{-18}
$\sigma_{2,6;1,6}^{(1)}$	0.57×10^{-18}
$\sigma_{2,5;2,4}^{(1)}$	4.05×10^{-18}
$\sigma_{2,5;1,5}^{(1)}$	0.66×10^{-18}
$\sigma_{1,6;1,5}^{(1)}$	4.51×10^{-18}
$\sigma_{1,6;0,6}^{(1)}$	0.32×10^{-18}
$\sigma_{2,4;2,3}^{(1)}$	3.97×10^{-18}
$\sigma_{2,4;1,4}^{(1)}$	0.77×10^{-18}
$\sigma_{1,5;1,4}^{(1)}$	4.57×10^{-18}
$\sigma_{0,6;0,5}^{(1)}$	5.06×10^{-18}
$\sigma_{1,4;1,3}^{(1)}$	4.54×10^{-18}
$\sigma_{0,5;0,4}^{(2)}$	5.20×10^{-18}
$\sigma_{1,5;0,5}^{(2)}$	1.00×10^{-52}
$\sigma_{2,3;2,2}^{(2)}$	5.00×10^{-51}
$\sigma_{2,3;1,3}^{(2)}$	1.00×10^{-50}
$\sigma_{1,4;0,4}^{(2)}$	5.00×10^{-51}
$\sigma_{2,2;2,1}^{(2)}$	1.00×10^{-52}
$\sigma_{2,2;1,2}^{(2)}$	1.00×10^{-51}
$\sigma_{1,3;1,2}^{(2)}$	1.00×10^{-51}
$\sigma_{1,3;0,3}^{(2)}$	1.00×10^{-49}
$\sigma_{0,4;0,3}^{(2)}$	1.00×10^{-51}
$\sigma_{2,1;2,0}^{(2)}$	1.00×10^{-52}
$\sigma_{2,1;1,1}^{(2)}$	1.00×10^{-52}
$\sigma_{1,2;1,1}^{(2)}$	1.00×10^{-52}
$\sigma_{1,2;0,2}^{(2)}$	1.00×10^{-52}
$\sigma_{0,3;0,2}^{(3)}$	2.20×10^{-50}
$\sigma_{2,0;1,0}^{(3)}$	1.00×10^{-84}
$\sigma_{1,1;1,0}^{(3)}$	1.00×10^{-84}
$\sigma_{1,1;0,1}^{(3)}$	1.00×10^{-84}
$\sigma_{0,2;0,1}^{(3)}$	5.00×10^{-81}
$\sigma_{1,0;0,0}^{(3)}$	1.00×10^{-84}
$\sigma_{0,1;0,0}^{(2)}$	1.00×10^{-84}
$\sigma_{2,6;2,4}^{(3)}$	1.00×10^{-52}
$\sigma_{2,6;2,3}^{(4)}$	1.00×10^{-84}
$\sigma_{2,6;2,2}^{(5)}$	3.00×10^{-117}
$\sigma_{2,6;2,1}^{(6)}$	6.00×10^{-150}
$\sigma_{2,6;2,0}^{(8)}$	5.00×10^{-183}
$\sigma_{2,6;1,0}^{(11)}$	4.00×10^{-249}
$\sigma_{2,6;0,0}^{(11)}$	1.00×10^{-348}

^(a) Single-photon cross-sections have been obtained from [10].

Table A2. Some near-resonant transitions for ionization of Neon at 93 eV as obtained from [10]. Note that this table is not by any means exhaustive.

Ion	Transition	Energy (eV)
Ne ³⁺	$(2s^2 2p^3)^4S_{3/2} \rightarrow (2s^2 2p^2 7d^1)^4P_{1/2}$	9.2896E+01
Ne ³⁺	$(2s^2 2p^3)^2P_{3/2} \rightarrow (2s^1 2p^3 3p^1)^2P_{1/2}$	9.3092E+01
Ne ³⁺	$(2s^1 2p^4)^4P_{3/2} \rightarrow (2p^4 3p^1)^4D_{5/2}$	9.2992E+01
Ne ⁴⁺	$(2s^1 2p^3)^1P_1 \rightarrow (2s^1 2p^2 4s^1)^1P_1$	9.2978E+01
Ne ⁴⁺	$(2s^2 2p^2)^3P_1 \rightarrow (2s^1 2p^2 3p^1)^3D_2$	9.2895E+01
Ne ⁴⁺	$(2s^1 2p^3)^3S_1 \rightarrow (2p^3 3p^1)^3P_2$	9.2836E+01
Ne ⁴⁺	$(2p^4)^3P_0 \rightarrow (2p^3 4s^1)^3D_1$	9.3176E+01
Ne ⁵⁺	$(2p^3)^2P_{1/2} \rightarrow (2p^2 3d^1)^2P_{1/2}$	9.3244E+01
Ne ⁶⁺	$(2p^2)^3P_2 \rightarrow (2p^1 20f^1)^3F_3$	1.8598E+02 ^(a)
Ne ⁶⁺	$(2p^2)^3P_2 \rightarrow (2p^1 20f^1)^3F_4$	1.8597E+02 ^(a)

^(a) Two photon transitions.